0013-7227/06/$15.00/0
Printed in U.S.A.

Endocrinology 147(12):5611–5623

doi: 10.1210/en.2006-0503

Insulin-Like Peptide 6: Characterization of Secretory Status and Posttranslational Modifications

Chunxia Lu, William H. Walker, Jinhong Sun, Ora A. Weisz, Robert B. Gibbs, Selma F. Witchel, Mark A. Sperling, Ram K. Menon

Department of Pediatrics (C.L., J.S., R.K.M.), University of Michigan, Ann Arbor, Michigan 48109; Departments of Cell Biology and Physiology (W.H.W., O.A.W.), Medicine (O.A.W.), and Pediatrics (S.F.W., M.A.S.), University of Pittsburgh School of Medicine, Pittsburgh, Pennsylvania 15213; and Department of Pharmaceutical Sciences (R.B.G.), University of Pittsburgh School of Pharmacy, Pittsburgh, Pennsylvania 15260

Insulin-like peptide 6 (Insl6) is a member of the insulin/relaxin superfamily with unknown biological function(s). In the current report, we establish that meiotic and postmeiotic germ cells of the testis are the principal sites of expression of Insl6. Analysis of stably or transiently transfected cells revealed that Insl6 is a secreted protein localized to the endoplasmic reticulum and Golgi. Secretion could be detected in both CHO and GC2 germ cells and was sensitive to brefeldin A treatment. In cell lysates, the predominant Insl6 band was approximately 28 kDa in size. In contrast, the predominant Insl6 species in the supernatant was 8 kDa in size, suggesting posttranslational processing of the precursor protein. Ectopically expressed Insl6 is processed and secreted in furin-deficient LoVo cells and in CHO cells treated with a furin inhibitor, although the size profile of the secreted protein is altered suggesting that Insl6 is a substrate for furin action. Furthermore, mutation of a putative furin cleavage site in the Insl6 peptide resulted in aberrant processing of the Insl6 peptide. Additional investigations of the structure of Insl6 protein provided evidence for posttranslational modifications of Insl6, including the presence of disulfide bonds, glycosylation, and ubiquitination. On the basis of the demonstrated secretory status of Insl6, we speculate that the physical proximity of the germ cell to the Sertoli cell renders the Sertoli cell a likely candidate for Insl6 action. (*Endocrinology* 147: 5611–5623, 2006)

THE INSULIN/IGF/relaxin family is an ancient family of functionally diverse proteins. Insulin or insulin-like proteins have been described in unicellular eukaryotes, primitive species such as insects, tunicates, annelids, and molluscans (1–6). Despite functional divergence within the family, all proteins of the insulin family exhibit a high degree of structural conservation. The primary peptide sequence of each member of the family is characterized by three domains comprised of an amino-terminal B peptide (or chain) joined to a carboxyl A peptide by an intervening C peptide (B-C-A) (7). Between the different hormones of the family and between species for a specific hormone, the B and A chain peptides are relatively invariant and exhibit a pattern of distinct and highly conserved cysteine motifs. These cysteine motifs characterize the family; specifically, the motif present in the A peptide has been termed the insulin signature. Many members of the insulin family of hormones are synthesized as preprohormones with the primary peptide undergoing posttranslational modification to generate a disulfide bond-linked heterodimer of the B and A peptides that functions as the active hormone.

At the beginning of the past decade, the insulin family was comprised of four members in mammals: insulin, IGF-I and IGF-II, and relaxin. Over the past decade additional members of the family termed insulin-like (INSL) 3 (8, 9), INSL4 (10, 11), INSL5 (12, 13), INSL6 (13–15), and INSL7 (16) have been identified. The precise biological role(s) of many of these new proteins, including Insl6 remains to be determined. Although previous studies had established that the testis is the site of maximum expression of Insl6, there is discordance among published studies as to the cell-type in the testis in which Insl6 is expressed. Hsu (13) localized expression to Leydig cells, whereas Lok *et al.* (15) concluded that Insl6 is expressed in pachytene spermatocytes and round spermatids but not in Leydig cells. At present, information regarding the secretory status, posttranslational modifications, and processing of Insl6 protein is lacking. The aims of this study were to determine the identity of the cell type-expressing Insl6 in the testis, to investigate the subcellular localization and secretory status of Insl6, and to identify and characterize potential posttranslational modifications and processing of this protein.

Materials and Methods

Cell culture

The culture media used for tissue culture experiments were obtained from Invitrogen (Carlsbad, CA) unless otherwise stated. Flp-In CHO cells (Invitrogen) and mInsl6-CHO cells were grown at 37 C in F12 medium supplemented with 10% fetal bovine serum (FBS). Germ cell (GC2), CRE8 cells, HEK293, and LoVo cells were grown in DMEM (4.5 g/liter glucose) with 10% FBS.

First Published Online August 24, 2006

Abbreviations: aa, Amino acid; BFA, brefeldin A; CI, cytotoxicity index; C_T, threshold cycle; Endo, endoglycosidase; ER, endoplasmic reticulum; FAM, 5-carboxyfluorescein; FBS, fetal bovine serum; FITC, fluorescein isothiocyanate; HRP, horseradish peroxidase; ISL, insulin-like peptide; PC, prohormone convertase; PNGase F, peptide *N*-glycosidase F.

***Endocrinology* is published monthly by The Endocrine Society (http://www.endo-society.org), the foremost professional society serving the endocrine community.**

Generation and characterization of anti-Insl6 antibody

Employing the services of a commercial vendor (BioSource International, Camarillo, CA), antimouse Insl6 sera were raised in the rabbit against keyhole hemocyanin-conjugated peptides termed EE and YV representing amino acid (aa) residues 56–71 and 134–150, respectively; both peptides overlap with the putative C peptide (14). The antisera were affinity purified against the homologous peptide using standard techniques. The specificity of the antibodies was verified by demonstrating that the homologous peptide (200 M excess) was able to block the detection of the Insl6 protein by Western blot analysis, whereas insulin failed to exhibit such competition (data not shown). In certain experiments, an anti-A chain mInsl6 antibody from Phoenix Pharmaceuticals (Belmont, CA) was used.

Animals

Eight-week-old male mice (C57BL) (Hilltop Laboratory Animals, Inc., Scottdale, PA) and testicular tissues from WBB6F1/J-Kit^{w}/Kit^{W-v} or WB/ReJ Kit^{w}/+ mice (The Jackson Laboratory, Bar Harbor, ME) were purchased. Female Sprague Dawley rats carrying pups at 19 d gestation were exposed to a single dose of whole-body x-ray irradiation equivalent to a dose of 200 rads using a ^{137}Cs source. Age-matched, nonirradiated females were employed as controls. The pups were born spontaneously on d 22 and killed 9 wk after birth. All experiments were carried in accordance with protocols approved by the Institutional Animal Care and Use Committees at the Children's Hospital of Pittsburgh, the University of Pittsburgh, or the University of Michigan.

Tissue collection

Euthanized animals were perfused with ice-cold saline followed by 4% paraformaldehyde in 50 mM sodium acetate (pH 6.5) and then with 4% paraformaldehyde in 50 mM Tris-HCl (pH 9.0). Testes were removed and postfixed in 4% paraformaldehyde in phosphate buffer (pH 7.2) at 4 C overnight. Testes were sequentially immersed at 4 C for 24-h periods in phosphate buffer (for paraffin embedding) or in 15% sucrose in phosphate buffer followed by 30% sucrose in phosphate buffer (for collecting frozen sections). Paraffin sections (10 μm), and frozen sections (20 μm) were cut and mounted onto Super Frost Plus glass slides (Fisher Scientific Co., Pittsburgh, PA). Paraffin sections were stored at room temperature and frozen sections were stored at −20 C before staining.

Staining

Paraffin sections were first deparaffinized with xylene and rehydrated with 50 mM PBS. Frozen sections were thawed in a desiccator at room temperature and then hydrated with 50 mM PBS. All sections were treated with 0.3% H_2O_2 in PBS for 15 min to inactivate endogenous peroxidase activity. Tissues were then rinsed with PBS, and primary antibody was applied at a dilution of 1:5000 or 1:10,000 in PBS containing 0.05% Triton X-100 and 5% normal goat serum. Control sections were either not exposed to the primary antibody or were treated with the primary antibody plus blocking peptide (10 μg/ml). Sections were incubated for 3 d at 4 C. Sections were then rinsed with PBS and treated with biotinylated goat-antirabbit IgG (3.0 μg/ml, Vector Laboratories, Burlingame, CA) for 3 h at ambient temperature. Sections were then rinsed with PBS. Antibody binding was visualized using the avidin-biotin-horseradish peroxidase (HRP) Elite system (Vector Laboratories). The avidin-biotin-HRP reagent was used at a concentration of 5 μl/ml each of reagent A and B in 50 mM PBS and incubated for 3 h at ambient temperature. Sections were reacted in a solution containing 3–3′ diaminobenzidine (0.5 mg/ml, Sigma-Aldrich, St. Louis, MO), 0.01% H_2O_2, and 0.03% NiCl in 50 mM Tris-HCl (pH 7.6) for 10 min. After antibody staining, sections were rinsed with PBS, some were counterstained with Mayers hematoxylin solution (Sigma-Aldrich), dehydrated with ethanol, cleared with xylenes, and cover slipped with DePeX (Gurr, BDH Laboratory Supplies, Poole, UK). For the tissues that were stained with Cy-3, the biotinylated secondary and avidin-biotin-HRP steps were omitted. Sections were incubated with Cy-3-labeled goat-antirabbit IgG (7.5 mg/ml; The Jackson Laboratory) in 50 mM PBS + 0.05% Triton for 1 h at room temperature. The sections were rinsed with 50 mM PBS, counterstained with Sytox Green (1:5000) for 5 min, and rinsed again with PBS. The sections were then rinsed briefly with water and overlaid with coverslips using Gel/Mount (Biomedia Corp., Foster City, CA) aqueous mounting media.

Plasmid construction and generation of Insl6-expressing stable cell line

The mInsl6-TOPO II and hInsl6-TOPO II constructs were generated by cloning murine or human Insl6 cDNA, respectively, into the TOPOII vector (Invitrogen). The plasmids encoding mInsl6 or hInsl6 fused at the C terminus to the myc-His tag were generated by subcloning Insl6 cDNA into the eukaryotic expression vector, pcDNA3.1(+) myc-his (Invitrogen). CHO cells stably expressing mInsl6 (mInsl6-CHO) were generated using the Flp-In system (Invitrogen) as per the manufacturer's protocol. Briefly, Insl6 tagged at the C terminus with the myc-his epitope was cloned into the Flp-In expression vector, pcDNA5/FRT. Flp-In CHO host cells were cotransfected with Insl6-myc-his pcDNA5/FRT and the Flp recombinase expression vector pOG44. Isogenic expression cell lines were isolated using hygromycin selection.

Recombinant adenovirus expressing murine Insl6

The myc-His epitope-tagged mouse Insl6 gene was subcloned into at the *Sma*I site of the pAdlox plasmid (Somatix Therapy Co., Alameda, CA) (17). Three micrograms each of the recombinant pAdlox plasmid and the ψ5 helper virus was transfected into Cre8 cells using Lipofectomine (Invitrogen). The culture medium was replaced every 2 d and the cells along with the media harvested in 7–8 d when the majority of the cells had rounded or detached. Cre8 cells were reinfected twice with the cell lysate to purify and amplify the recombinant virus (Ad-mInsl6). Virus titer was determined by plaque assay in HEK293 cells.

Production of recombinant mInsl6 with mutation in putative furin cleavage site

The putative furin cleavage motif (RKRR) in mInsl6 peptide located between aa 162 and 165 was mutated (to AAAA) using the QuickChange Site-Directed Mutagenesis Kit (Stratagene, La Jolla, CA) according to the manufacturer's instructions.

Immunofluorescence staining

mInsl6-CHO stable cells or Ad-mInsl6-infected GC2 cells were fixed with 4% paraformaldehyde and permeabilized with 0.1% Triton X-100. Double staining with rabbit or mouse anti-myc (1:100 dilution) and rabbit anti-Grp78 (1:100) or mouse GM130 (1:100) antibody was visualized by fluorescein isothiocyanate (FITC)-labeled antimouse IgG and Rhodamine-labeled antirabbit IgG. Cells were observed using a confocal microscope (Olympus FluoView 500, Olympus, Tokyo, Japan) or a Nikon TE200 Eclipse fluorescence microscope (Nikon, Tokyo, Japan). In certain experiments, the cells were exposed to nocodazole (20 μM for 60 min on ice) before fixation and immunofluorescence staining.

Transient transfection

CHO cells (0.4×10^6) were plated on 35-mm plates 24 h before transfection. Plasmid DNA (3 μg) was transfected per plate using the Lipofectamine method (Invitrogen). After 6 h of incubation, the DNA-Lipofectamine mixture was removed and then supplemented with medium for 48 h before harvest for Western blot analysis.

Infection of GC2 cells with Ad-mInsl6

GC2 cells were infected with Ad-mInsl6 at 30 plaque-forming units/cell. In indicated experiments, infected cells or supernatant from the infected cells were harvested after 48 h of exposure of the cells to either brefeldin A (BFA) or vehicle.

Deglycosylation assay

Protein extracts [lysed in radioimmunoprecipitation assay buffer containing 50 mM Tris-HCl (pH 7.5), 150 mM NaCl, 2 mM EGTA and 0.1% Triton X-100] from CHO cells transiently transfected with Insl6 express-

ing plasmid or GC2 cells infected with Ad-mInsl6 were treated with peptide *N*-glycosidase F (PNGase F) or endoglycosidase (Endo) H (New England Biolabs, Beverly, MA) according to the manufacturer's protocol. For PNGase F treatment, a 10-μl aliquot of protein was mixed with 1 μl 10× denaturation buffer and boiled for 10 min. The denatured protein mixture was mixed with 1 μl 10× reaction buffer, 1 μl 10% NP 40, and 1 μl PNGase F. The reaction was carried out at 37 C for 1–4 h. For Endo H treatment, 30-μg aliquots of protein extracts were denatured with 1× glycoprotein denaturing buffer at 100 C for 10 min and then treated with 500 U Endo H in the presence of 1× reaction buffer [50 mM sodium citrate (pH 5.5)] for 1 h at 37 C. The reactions were stopped by boiling in sodium dodecyl sulfate sample buffer at 100 C for 5 min and analyzed by SDS-PAGE.

Western blot analysis

CHO or LoVo cells transiently transfected with Insl6 plasmid construct or CHO cells stably expressing Insl6 were harvested at indicated time points. GC2 cells infected with Ad-mInsl6 were harvested after 48 h of infection. BFA (Sigma-Aldrich) treatment was performed by exposing cells to BFA (1–50 μg/ml) for the indicated time periods. Cells were washed twice with cold PBS, lysed in radioimmunoprecipitation assay buffer [50 mM Tris-HCl (pH 7.5), 150 mM NaCl, 2 mM EGTA, and 0.1% Triton X-100] supplemented with a protease inhibitor cocktail (Roche Diagnostics, Indianapolis, IN), supernatant precipitated with 15% trichloroacetic acid, and the protein pellet resuspended in 1% sodium dodecyl sulfate. Equal amounts protein were size-fractionated via SDS-PAGE and subjected to Western blot analysis as previously described (18). The primary antibodies used in these analyses were anti-myc (9E10, Santa Cruz Biochemicals, Santa Cruz, CA) routinely used at a dilution of 1:500. All results are representative for three or four independent experiments.

Lactate dehydrogenase activity assay

Cytotoxicity was determined using a cytotoxicity detection kit (Roche Diagnostics). Briefly, 100 μl supernatant aliquot was mixed with 100 μl reaction mixture and incubated for 20 min at room temperature. Low and high controls for the assay were established by assaying the cell culture medium and the supernatant of Triton X-100-treated cells, respectively. The cytotoxicity index (CI) was determined by the equation: CI = (sample − low control)/(high control − low control) × 100.

In vitro *transcription and translation*

Transcription and translation coupled reticulocyte lysate and wheat germ extract systems were purchased from Promega (Madison, WI). The reactions were initiated by mixing 3 μg Insl6-TOPO II plasmid DNA with 50 μl reticulocyte lysate or wheat germ extract reaction mixtures in the presence of [^{35}S] cysteine (MP Biomedicals, Irvine, CA) and T7 polymerase. After incubation at 30 C for 90 min, the products were size-fractionated via electrophoresis through a 14% SDS-PAGE gel. In some reactions, His-ubiquitin (Sigma-Aldrich) was added at the initiation of the reaction (19). Where indicated, the intensity of the specific bands was quantitated by densitometry (Bio-Rad, Hercules, CA).

RNA extraction

Total RNA was extracted from testes either via a guanidine isothiocyanate-based technique followed by cesium chloride gradient purification or by using TRI-Reagent (Molecular Research Center, Cincinnati, OH) (20).

Real-time RT-PCR assay

Real-time quantitative RT-PCR using the ABI Prism 7700 Sequence Detection System (PE Biosystems, Foster City, CA) was carried out using established protocols (21). The primers (synthesized by Invitrogen) and TaqMan probes (synthesized by PE Biosystems) for the quantitation of the Insl6 and LH receptor transcripts were designed using the primer design software Primer Express (PE Biosystems) (Table 1). The primers and TaqMan probe for 18S rRNA were purchased from a commercial vendor (PE Biosystems). The 18S probe was labeled with the reporter fluorescent dye VIC and the Insl6 and LH receptor probes with the reporter dye 5-carboxyfluorescein (FAM). The relative efficiencies of the Insl6 and LH receptor primers/probe sets and the 18S primer/probe pair were tested by subjecting serial dilutions of a single RNA sample from each of the tissues analyzed to real-time RT-PCR analysis. The plot of log input *vs.* Δ Threshold cycle (C_T) was less than 0.1, which satisfies the previously established criterion for equivalence of efficiency of amplification (22). After confirming that the efficiency of amplification of the gene of interest (*e.g.* Insl6) and 18S transcripts were approximately equal, the amount of the transcripts for the specific gene relative to the 18S transcript was determined by using the comparative C_T (separate tube) method (22). Briefly, 5-ng aliquots of total RNA were analyzed using the One-Tube RT-PCR protocol (PE Biosystems). After RT at 48 C for 30 min, the samples were subjected to PCR analysis using the following cycling parameters: 95 C for 10 min and 95 C for 15 sec → 60 C for 1 min for 40 cycles. Each sample was analyzed in triplicate in individual assays performed on two or more occasions.

Results

Cellular localization of Insl6 in mouse testis

Two strategies were used to determine the cellular localization of Insl6 expression in the rodent testis.

Immunocytochemistry. For purposes of immunostaining with anti-Insl6 antibody, we evaluated both paraffin and frozen testis sections. The staining observed under both conditions was similar with the exception that staining of the frozen sections tended to be denser. Using an antipeptide antibody (EE) directed against an epitope of the Insl6 encompassing contiguous portions of the B and C chains of the Insl6 molecule, we observed staining of the germ cells of the testis. The germ cells stained with the Insl6 antibody were mid-pachytene spermatocytes, secondary spermatocytes, and round spermatids (Fig. 1A). Preincubation of the antibody

TABLE 1. Sequence of primer probe sets used in the real-time RT-PCR assay

	Primer/probe	Sequence
Mouse Insl6	Forward	TCACGCAAGGGCAAAGC
	Reverse	GGGACTGGGTTTGTGAATCTTC
	Probe (FAM)	AACCCTCACCCTTCTTCCTCCGCCT
Rat Insl6	Forward	CCCAACTATCAGCTTAAAAAGGA
	Reverse	CGCTGAAGGTACTCATTTTGTCA
	Probe (FAM)	CATTCATACCACGGTGGCAAGCCC
Rat LHR	Forward	ACATTGAACCTGGTGCTTTTACAA
	Reverse	AGGGTTCGGATGCCTGTG
	Probe (FAM)	CCTCCCTCGGTTAAAATACCTGAG CATCTGTA
18S	Primers	Proprietary (Applied Biosystems, Foster City, CA)
	Probe (VIC)	Proprietary (Applied Biosystems)

5′-End reporter dyes, FAM and VIC (proprietary; Applied Biosystems). The quencher fluorescent dye at the 3′-end was 5-carboxytetramethylrhodamine for all probes.

with the homologous peptide abrogated the staining indicating that the observed staining was specific (Fig. 1B). Counterstaining with a nucleus-specific stain (Sytox green, Invitrogen) indicated that in germ cells, Insl6 was excluded from the nucleus and was localized to the cytoplasmic region (Fig. 1C). No specific staining of either Leydig or Sertoli cells was detected. Similar results (data not shown) were observed with an antipeptide antibody (YV) directed against a second epitope of the murine Insl6 protein.

Effect of germ cell aplasia on Insl6 expression. Irradiation of the fetal testis results in preferential loss of germ cells in postnatal life. We exploited this model to investigate the cellular localization of Insl6 in the rat testis. Using a real-time quantitative RT-PCR technique, we measured the steady-state abundance of Insl6 mRNA in the testis of 9-wk-old male rats that had been subjected to irradiation during fetal life. The expression of Insl6 in the testis of the irradiated rats was 10–20% of age-matched nonirradiated controls (Fig. 2A). To validate the model for preferential loss of germ cells, we measured the levels of the Leydig cell-specific LH receptor mRNA in these samples. The abundance of the LH receptor mRNA in the testis of the rats exposed to radiation *in utero* was increased. This increase in the steady-state abundance of LH receptor RNA reflects the relative enrichment of testicular tissue for Leydig cells after the radiation-induced loss of the germ cell, which is the predominant cell type in the mature testes. Hence, these results confirm the relative sparing of the Leydig cell in this model. Insl6 mRNA expression was also undetectable in the testis of mice with germ cell aplasia due to a mutation in the *kit* oncogene (WBB6F1/J-$Kit^{W}/Kit^{W\text{-}v}$) (Fig. 2B). Thus, in the absence of germ cells, despite the presence of Leydig cells, Insl6 mRNA was essentially undetectable in the testis.

Expression of Insl6

Ontogeny of expression of Insl6 in mouse testis. Real-time RT-PCR assay was used to characterize the ontogenic profile of expression of Insl6 in mouse testis. Insl6 mRNA expression was detectable at low levels at embryonic d 14.5 and 17.5, and the level of expression remained low (0 and 7 d postnatal) until postnatal d 20, when there was a 40- to 50-fold increase in Insl6 mRNA abundance with maximum levels attained by 40 d and maintained up to 90 d of age (Fig. 3A). Notably, pachytene spermatocytes, identified in our studies as a major site of expression of Insl6, first appear in the mouse testis around postnatal d 20.

Expression of Insl6 in other mouse tissues. Real-time RT-PCR assay was used to characterize the quantitative profile of expression of Insl6 in various mouse tissues. Although Insl6 mRNA expression was most abundant in the testis, Insl6 mRNA was also detected in intestine, thymus, kidney, uterus, ovary, spleen, breast, lung, and liver. However, the level of expression in these tissues was only 1–8% of that observed in the testis (Fig. 3B). Steady-state abundance of Insl6 mRNA in GC2 cells, a murine germ cell line, was also only 1% of that measured in the intact mouse testis (data not shown).

Intracellular localization of Insl6. The subcellular localization of Insl6 was investigated by colocalization studies of both CHO cells stably expressing either mInsl6 or hInsl6 and GC2 cells expressing adenoviral-mediated mInsl6. Staining with antibodies directed against Bip (Fig. 4A) and GM130 (Fig. 4B) proteins as marker for the endoplasmic reticulum (ER) and the Golgi apparatus, respectively, revealed that in both CHO and GC2 cells, Insl6 protein colocalized to the perinuclear ER region and to the Golgi apparatus. Furthermore, exposure of the cell to nocodazole, a reagent that disrupts microtubules and causes fragmentation of the Golgi apparatus, revealed that there was parallel redistribution of GM130 and Insl6, indicative of localization of Insl6 to the Golgi apparatus (Fig. 4B).

Posttranslational processing and modifications of Insl6

At present, information about the biological role(s) of Insl6 is not available. As a first step toward identification of the

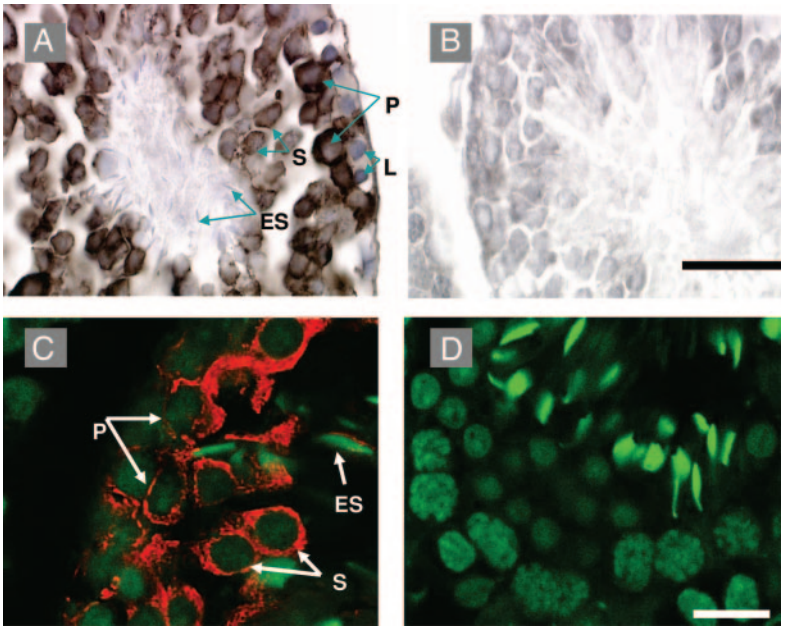

FIG. 1. Immunohistochemical detection of Insl6 expression in germ cells of the testis. Insl6 expression in testicular section from mice (8 wk old) using anti-Insl6 antibody (EE) without (A and C) and with (B and D) presaturation with antigen peptide (×200). The binding of the primary antibody was either visualized by light microscopy using the avidin-biotin HRP methodology (A and B) or via confocal microscopy of sections labeled with Cy-3-conjugated secondary antibody (C and D). The slides were also counterstained with either hematoxylin (A and B) or Sytox green (C and D). The specific stainings of leptotene spermatocytes (L), pachytene spermatocytes (P), spermatids (S), and elongated spermatids (ES) are indicated by *solid arrows*. The results are representative of two or more independent experiments. *Scale bar*, 25 μm in A and B; *scale bar*, 10 μm in C and D.

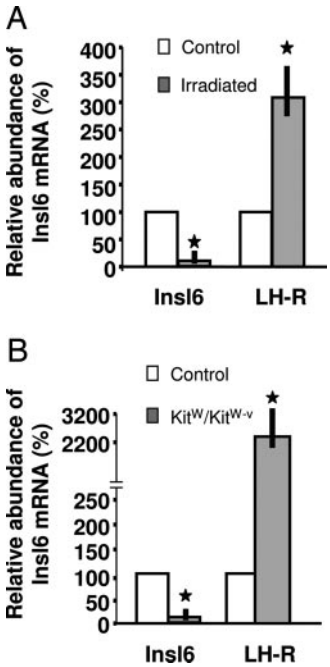

FIG. 2. Effect of germ cell aplasia on Insl6 mRNA and protein expression. A and B, Steady-state abundance of Insl6 mRNA was measured by real-time quantitative RT-PCR assay in testis of rats (A) or mice (B) (n = 3–7). The abundance of LH receptor mRNA was assayed as a marker of germ cells. A, Rats exposed to radiation during fetal life compared with nonexposed control rats. B, Germ cell aplasia mice WBB6F1/J-Kit^{W}/Kit^{W-v} compared with the control mice, WB/ReJ Kit^{w}/+. The values are represented relative to level of expression in the vehicle-treated group and are depicted as mean and range. The range is determined by evaluating the expression $2^{-\Delta\Delta}C_T$ with $^{\Delta\Delta}C_T + s$ and $^{\Delta\Delta}C_T - s$, where s is the SD of the $^{\Delta\Delta}C_T$ value (22). *, $P < 0.01$ compared with the control group by ANOVA.

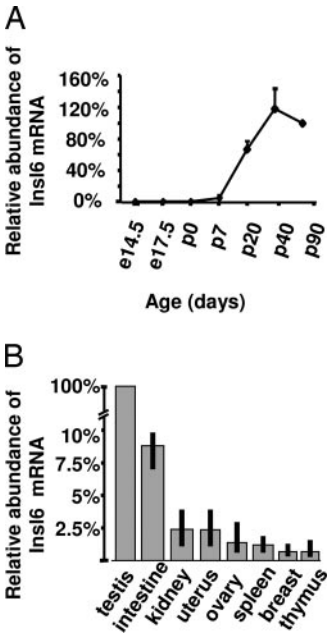

FIG. 3. Insl6 expression: ontogeny and tissue distribution. A, Ontogeny of Insl6 expression in mouse testis. Expression of Insl6 mRNA was measured by real-time quantitative RT-PCR assay in testis of mice (n = 3–5) at indicated ages. The values (mean ± SE) are represented as relative to level of Insl6 mRNA at 90 d designated as 100%. e, embryonic; p, postnatal. B, Tissue-specific expression of Insl6. Insl6 mRNA levels were measured by real-time quantitative RT-PCR assay in the indicated tissues of adult (6–8 wk old; n = 3–5) male (small bowel, kidney, spleen, and thymus) or female (uterus and breast). The levels are depicted as relative to Insl6 abundance in testis designated as 100%. The results are depicted as mean and range. The range is determined by evaluating the expression, $2^{-\Delta\Delta}C_T$ with $^{\Delta\Delta}C_T + s$ and $^{\Delta\Delta}C_T - s$, where s is the SD of the $^{\Delta\Delta}C_T$ value (22).

putative biological role(s) of Insl6, we analyzed the Insl6 protein for posttranslational processing and modifications.

Insl6 is a secreted protein. Based on the knowledge that canonical members of the insulin family are secreted proteins, the possibility of Insl6 being a secreted protein was tested by analyzing the supernatant of CHO cells stably transfected with mInsl6 (mInsl6-CHO) and GC2 cells infected with adenovirus expressing mInsl6 (Ad-mInsl6). As shown in Fig. 5, mouse Insl6 protein could be detected in the supernatant of both cell types, supporting the hypothesis that Insl6 is a secreted protein. In contrast to the cell lysate where the predominant species was 28 kDa in size (*top*), in the cell culture supernatant, a substantial fraction of the secreted Insl6 was 8 kDa in size (*bottom*). A similar size profile of Insl6 protein was also observed in CHO cells transiently transfected with mInsl6 (data not shown). These results suggest that the 8-kDa form represents a processed form of the precursor 28-kDa species of mInsl6.

To examine the possibility that Insl6 protein in supernatant was released from the lysis of dead cells, we investigated the effect of BFA, a yeast metabolite that blocks protein translocation from ER to Golgi, on Insl6 secretion in mInsl6-CHO (Fig. 6A) and Ad-mInsl6-infected GC2 cells (Fig. 6B). These results demonstrate that BFA inhibited the secretion of Insl6 (the 8 kDa band) into the cell culture supernatant (Fig. 6, A, *top*, and B). This dose-dependent effect of BFA in both CHO and GC2 cells supports the conclusion that Insl6 is secreted into the medium, and the presence of Insl6 in the cell culture supernatant is not the result of lysis of dead cells. Analysis of the whole-cell lysates (Fig. 6A, *bottom*) verified that BFA did not inhibit the synthesis of the 28-kDa Insl6 precursor, supporting the conclusion that the observed BFA-dependent decrease in Insl6 in the cell culture supernatant was not the result of decreased synthesis of the Insl6. To obtain a quantitative measure of cell lysis, we assayed the cell culture medium from mInsl6-CHO for lactate dehydrogenase activity (an index of cell death) and calculated the CI. These results indicate that there were no significant changes in the CI in the transfected cells (10–12%) compared with the untransfected cells (9–10%), further supporting the secretory status of the Insl6 protein in these model systems. In contrast, adenoviral infection of GC2 cells resulted in a limited degree of cell death. In this context, the 28-kDa band detected by Western blotting of the cell supernatant of GC2 expressing adenovirally expressed Insl6 (Fig. 6B) possibly represents Insl6 precursor released from the lysis of the dead cells. This scenario would also be compatible with the observed insensitivity of the 28-kDa band to treatment with BFA (Fig. 6B).

Insl6 is a target for processing by furin. In silico analysis of the primary structure of the mInsl6 aa sequence indicated the presence of a single furin recognition motif (RKRR) at aa

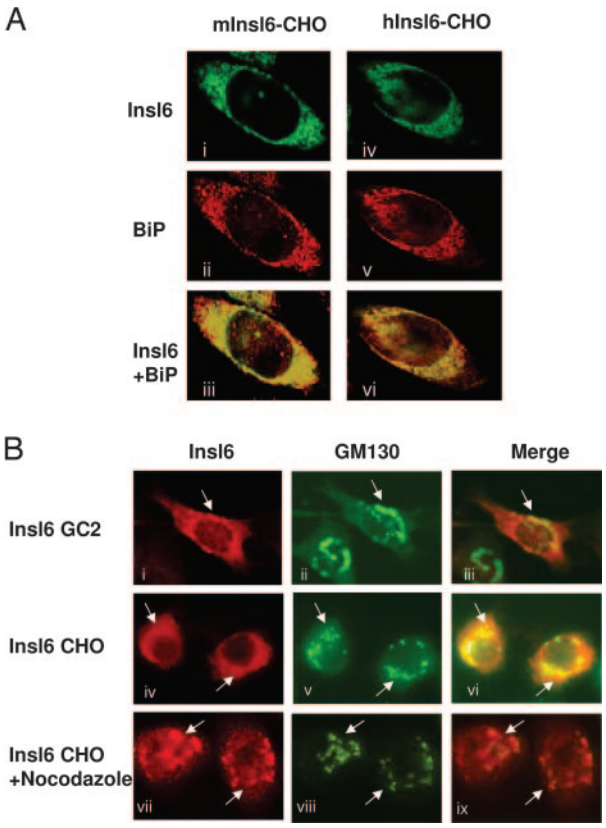

FIG. 4. Subcellular localization of Insl6 by coimmunofluorescence. A, CHO cells stably expressing either c-*myc*-tagged mInsl6 (i–iii) or hInsl6 (iv–vi) were fixed, permeabilized, and incubated with primary antibodies, mouse anti-myc, or rabbit anti-Bip. The specific binding of the primary antibodies was detected by using FITC-labeled antimouse IgG or rhodamine-labeled antirabbit IgG, respectively. Immunofluorescence staining for Insl6 (i and iv) and the ER marker Bip 78 (ii and v) depict identical patterns as illustrated in the *merged* panels (iii and vi). The results are representative of three or more independent experiments. B, GC2 cells exhibiting adenovirus-mediated mInsl6 expression (i–iii) or CHO cells stably expressing c-*myc*-tagged mInsl6 (iv–ix) were fixed, permeabilized, and incubated with primary antibodies, rabbit anti-myc, or mouse anti-GM130. The specific binding of the primary antibodies was detected by using FITC-labeled antimouse IgG or rhodamine-labeled antirabbit IgG, respectively. Immunofluorescence staining for Insl6 (i and iv) and the Golgi marker GM 130 (ii and v) depict overlapping patterns as illustrated in the *merged* panels (iii and vi). To further demonstrate the Golgi localization of Insl6, mInsl6-CHO cells were exposed to nocodazole (vii–ix) before fixation and immunofluorescence staining for Insl6 (vii) and the Golgi marker GM130 (viii) as described above. The disruption of Golgi by nocodazole and consequent parallel redistribution of GM 130 and Insl6 are illustrated in the *merged* panel (ix). The results are representative of two independent experiments.

162–165. To investigate the role of furin in the posttranslational processing of the Insl6 protein, furin-deficient LoVo cells were transfected with wild-type mInsl6 or a mutant mInsl6 peptide in which the putative furin-preferred consensus sequence RKRR was mutated to AAAA (Fig. 7). Although secretion of mInsl6 was intact in the LoVo cells, the size pattern of the secreted proteins was altered in these cells. Thus, in LoVo cells transfected with wild-type mInsl6, a single protein band of approximately 8 kDa was detected in contrast to two bands of 8 and 6 kDa detected from mInsl6-CHO cells (Fig. 7, *upper*). Similar results were also obtained

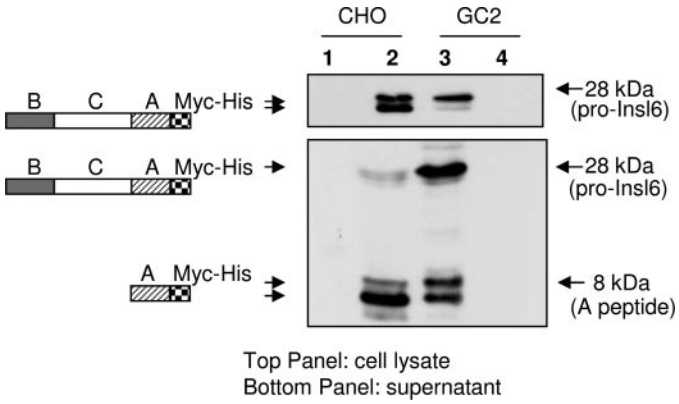

FIG. 5. Insl6 is a secreted protein. Naïve CHO cells (lane 1), CHO cells stably expressing c-*myc*-tagged mInsl6 (lane 2), Ad-mInsl6-infected GC2 (lane 3), or naïve GC2 cells (lane 4) were maintained overnight in DMEM supplemented with 2% FBS. The cells (*top*) and culture medium (*bottom*) were harvested separately and processed for analysis. Approximately 2% of whole-cell lysate (*top*) and 20% of the concentrated culture medium (*bottom*) (from 35-mm culture plate) was subjected to SDS-PAGE size fractionation under reducing conditions and Western blot analysis with anti c-*myc* antibody for the presence of the Insl6 protein. The predicted compositions of the various Insl6 bands and the positions of the molecular mass marker are indicated.

by treating mInsl6-CHO cells with the furin inhibitor Dec-RVKR-CMK (Fig. 7, *lower*). Complementation of LoVo cells via ectopic expression of furin reverted the secretion pattern of mInsl6 to that observed in CHO wild-type cells with the appearance of the 8- and 6-kDa bands (Fig. 7, *upper*, lane 4). These results indicate that furin plays a role in the processing of the Insl6 prohormone. Furthermore, the molecular size of the secreted mutant mInsl6 increased to approximately 16 kDa in both CHO (Fig. 7, *upper*, lane 2) and LoVo (Fig. 7, *upper*, lane 6) cells, indicating that the RKRR sequence is the target for action of both furin and a nonfurin prohormone convertase (PC) and is essential for the complete processing of the Insl6 peptide.

Insl6 is linked by disulfide bonds. The primary structure of B and A peptides of mInsl6 reveal conserved cysteine motifs that are a hallmark of the insulin/relaxin protein superfamily. To investigate whether these cysteine motifs result in the formation of intra-/intermolecular disulfide bonds in mInsl6 protein, cell lysates (Fig. 8A, *top*) or supernatants (Fig. 8A, *bottom*) of mInsl6-CHO stable cells were size-fractionated through a 15% PAGE gel under either nonreducing or reducing conditions and then subjected to Western blot analysis. In cell lysates (Fig. 8A, *top*), mInsl6 migrated at a faster rate in the nonreducing (lanes 1 and 2) compared with reducing milieu (lanes 3–6). These results are compatible with the presence of intramolecular disulfide bonds in the precursor species. In contrast, in the cell culture supernatant (Fig. 8A, *bottom*) under nonreducing conditions (lane 2), the size of secreted mInsl6 was larger (14–16 kDa) compared with the size observed with reducing condition (8 kDa) (lanes 3–5). These findings can be explained by a model of mInsl6 characterized by the presence of intermolecular disulfide bonds linking B and A peptides, the 14–16-kDa species representing the B and A disulfide-linked secreted Insl6 protein

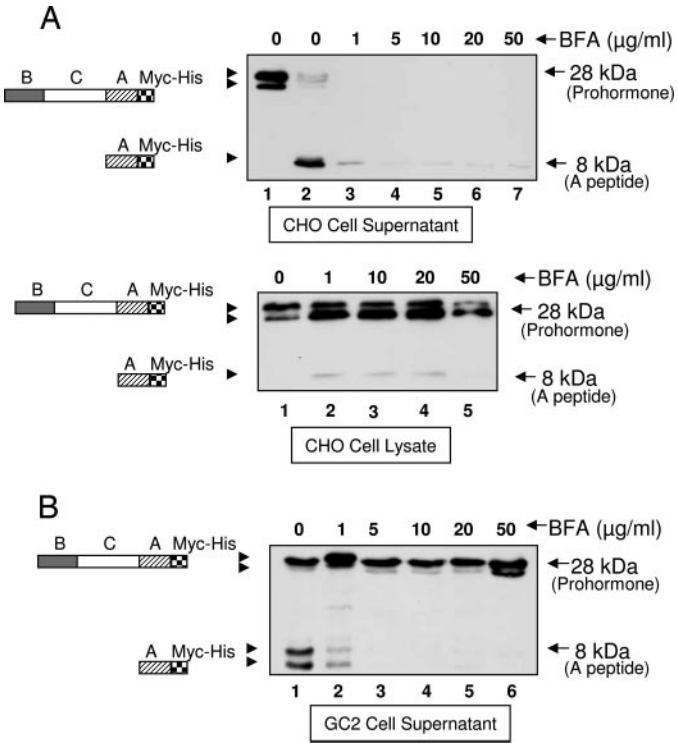

FIG. 6. Secretion of Insl6 is sensitive to BFA treatment. A, CHO cells stably expressing c-*myc*-tagged mInsl6 were treated with BFA at the indicated concentration for 6 h, and the culture medium (*top*, lanes 2–7) and cells (*top*, lane 1; *bottom*, lanes 1–5) were harvested separately and processed for analysis. Approximately 20% of the culture medium from culture plate (35 mm) was subjected to SDS-PAGE size fractionation under reducing conditions and Western blot analysis with anti c-*myc* antibody for the presence of the Insl6 protein. The predicted compositions of the various Insl6 bands and the positions of the molecular mass marker are indicated. B, Insl6-adenovirus (Ad-mInsl6)-infected GC2 cells were treated with BFA at the indicated concentration overnight, and the culture medium was harvested and processed for analysis. Approximately 20% of the concentrated culture medium (from 35-mm culture plate) was subjected to SDS-PAGE size fractionation under reducing conditions and Western blot analysis with anti c-*myc* antibody for the presence of the Insl6 protein. The predicted compositions of the various Insl6 bands and the positions of the molecular mass marker are indicated.

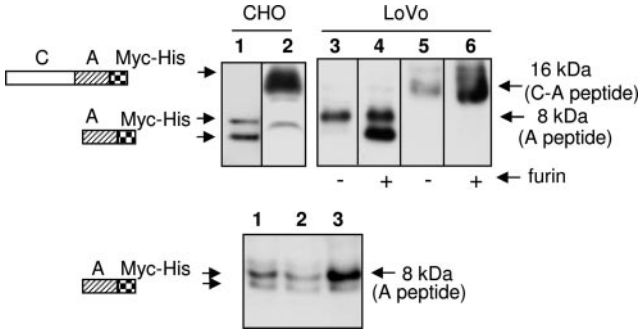

FIG. 7. Insl6 is a target for processing by furin. *Top*, Processing of Insl6 protein in CHO and furin-deficient LoVo cells. Supernatants of CHO cells stably expressing c-*myc*-tagged mInsl6 (lane 1), CHO cells transiently transfected with furin cleavage site mutant mouse c-*myc*-tagged Insl6 (lane 2), LoVo cells transiently transfected with wild-type mouse c-*myc*-tagged Insl6 (lanes 3 and 4), or LoVo cells transiently transfected with furin cleavage site mutant mouse c-*myc*-tagged Insl6 (lanes 5 and 6) in the absence (lanes 3 and 5) or presence (lanes 4 and 6) of ectopic expression of human furin were size-fractionated by SDS-PAGE under reducing conditions and analyzed by Western blot analysis with anti c-*myc* antibody for the presence of the Insl6 protein as described in *Materials and Methods*. Approximately 20% of the culture medium from each transfection was subjected to this analysis. The predicted compositions of the various Insl6 bands and the positions of the molecular mass marker are indicated. *Bottom*, Processing of Insl6 protein in the presence of furin inhibitor Dec-RVKR-CMK. CHO cells stably expressing c-*myc*-tagged mInsl6 were cultured in 2% serum and treated with 25 μM furin inhibitor Dec-RVKR-CMK for 24 h (lane 3). Control cells were treated with equal amount of solvent (methanol, lane 2) or without methanol (lane 1). Approximately 20% of the culture medium (from 35-mm culture plate) was subjected to SDS-PAGE size fractionation and Western blot analysis with anti c-*myc* antibody for the presence of the Insl6 protein. The predicted compositions of the various Insl6 bands and the positions of the molecular mass marker are indicated.

and the 8-kDa species representing the epitope-tagged A peptide.

We next investigated whether the human Insl6 protein also exhibited a similar secondary/tertiary structure. In contrast to the murine peptide, there was no alteration in the electrophoretic mobility of the 10-kDa secreted human peptide in reducing *vs.* nonreducing conditions (Fig. 8B). This observation, obtained in both CHO (Fig. 8B) and LoVo (data not shown) cells, suggests the absence of disulfide bonds (and hence of the B peptide) in the secreted hInsl6 peptide. An alternate explanation is that the absence of the B peptide in the secreted hInsl6 protein is due to aberrant processing of hInsl6 and is an artifact of the cell culture models (CHO and LoVo cells) employed.

Differential N-*linked glycosylation of murine and human Insl6 proteins.* An *in silico* analysis of the primary structure of the human and murine Insl6 protein sequence using the NetNGly 1.0 software program (http://www.cbs.dtu.dk/services) predicted the presence of a single *N*-linked glycosylation site (at residue 49 in the human and residue 158 in the mouse). This prediction was tested by analyzing the effect of PNGase F on the electrophoretic mobility of recombinant Insl6 proteins in cell lysate. The electrophoretic mobility of the murine prepro/pro-Insl6 protein in cell lysates was unaffected (Fig. 9A, *bottom*). In contrast, the electrophoretic mobility of the human prepro/pro-Insl6 peptide was increased by treatment of cell lysates with PNGase F, suggesting that the human protein is modified by *N*-linked glycosylation (Fig. 9A, *upper*). However, we were unable to confirm that the secreted hInsl6 peptide is also glycosylated. This is because the predicted glycosylation site on the hInsl6 peptide is located on the putative B peptide, and as detailed in the prior section, we were unable to detect the presence of the B peptide in the secreted hInsl6 peptide. To exclude the possibility that CHO is not an appropriate model system to investigate the glycosylation status of Insl6, we subjected Insl6 ectopically expressed in GC2 to similar analysis. These results (Fig. 9B) verified the presence of *N*-linked glycosylation in human prepro- or pro-Insl6 and its absence in the murine protein. To further characterize the nature of the glycosylation of the human Insl6 precursor, we tested the effect of Endo H on recombinant human Insl6 protein. The human Insl6 protein was susceptible to Endo H treatment, indicating the presence of immature high mannose residues (Fig. 9C). We confirmed the lack of effect of Endo F on mouse

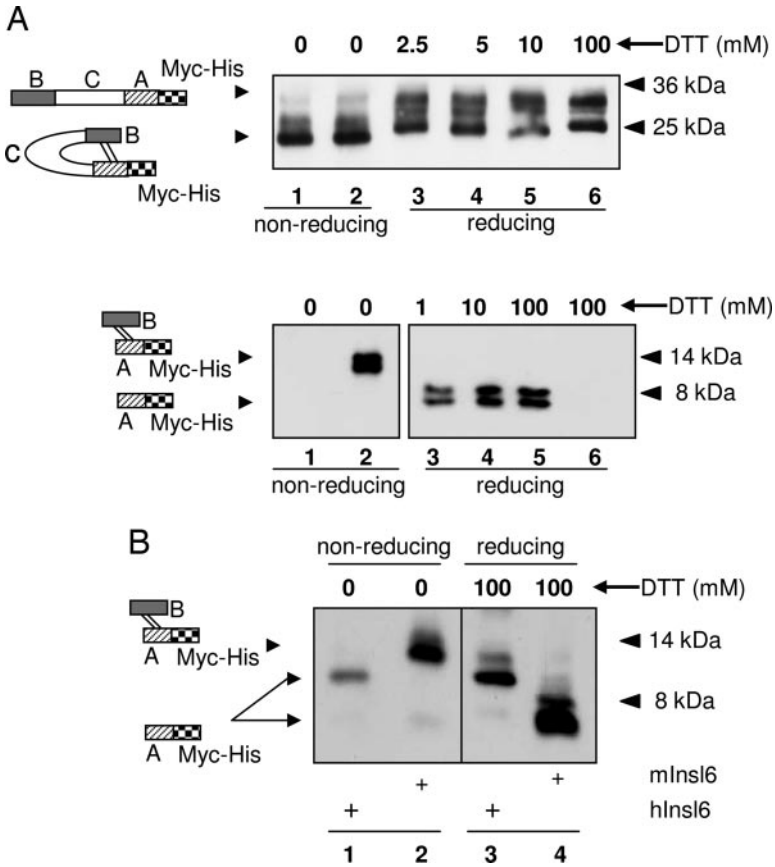

FIG. 8. Presence of disulfide bonds in Insl6. A, Intramolecular disulfide bonds in mouse Insl6. Whole-cell lysates (*top*) or cell culture supernatant (*bottom*) of CHO cells stably expressing c-*myc*-tagged mInsl6 protein (mInsl6-CHO; lanes 1–6, *top*; and lanes 2–5, *bottom*) or untransfected CHO cells (*bottom*, lanes 1 and 6) were size-fractionated by SDS-PAGE electrophoresis under either nonreducing conditions (*top*, lane 1, nonboiled, lane 2, boiled; *bottom*, lanes 1 and 2, nonboiled) or reducing conditions (dithiothreitol, 1–100 mM, lanes 3–6, *top* and *bottom*). The electrophoretic mobility of the Insl6 protein was analyzed by Western blot analysis using anti c-*myc* antibody. The predicted compositions of the various Insl6 bands and the positions of the molecular mass marker are indicated. B, Differences in disulfide bond formation between mouse and human Insl6 proteins. Cell culture supernatant of CHO cells expressing c-*myc*-tagged human (lanes 1 and 3) or mInsl6 protein (lanes 2 and 4) were size-fractionated by SDS-PAGE electrophoresis under either nonreducing conditions (lane 1 and 2) or reducing conditions (100 mM dithiothreitol, lanes 3 and 4). The electrophoretic mobility of the Insl6 protein was analyzed by Western blot analysis using anti c-*myc* antibody. The predicted compositions of the various Insl6 bands and the positions of the molecular mass marker are indicated.

Insl6 by examining mouse testis extracts (Fig. 9D, *top*). To ascertain the specificity of the anti-Insl6 antibody used to detect endogenous Insl6 in mouse testes, we tested two anti-mInsl6 peptide antibodies, custom-made EE antibody directed against the C chain (Fig. 9D, *top*) and the commercially available anti-A chain antibody (Phoenix Pharmaceuticals; Fig. 9D, *bottom*). Western blot analysis of intact testes and primary germ cell extracts with either of these antibodies revealed the presence of a 24-kDa doublet band compatible with prepro- or pro-Insl6 protein. In contrast, a specific signal was not detected in liver extracts. In addition to the 24-kDa doublet, bands that migrated at 15 and 30 kDa were observed when testis extracts were blotted with the EE antibody. The identity of these bands is not clear at the present time. The 15-kDa band could represent a B-C chain intermediate form of Insl6. The 30-kDa band is possibly nonspecific because this band was not observed in germ cell extracts blotted with the anti-A peptide antibody.

Insl6 is ubiquinated. To investigate whether Insl6 can be subjected to other posttranslational modification such as ubiquination, recombinant mInsl6 protein was synthesized *in vitro* by coupled transcription and translation reaction using either rabbit reticulocyte lysate or wheat germ extract systems. In addition to the full-length protein, the mInsl6 protein produced with the reticulocyte lysate, but not the wheat germ lysate, exhibited bands of higher molecular mass (lane 2, Fig. 10A). These higher molecular mass bands were spaced at approximately 8-kDa intervals. A similar profile was observed with the recombinant human Insl6 protein (data not shown). The spacing of the bands suggested the possibility that the Insl6 protein could be ubiquinated. To confirm this hypothesis, the coupled transcription and translation reaction in the reticulocyte lysate system was carried out in the presence of His-tagged ubiquitin (lane 3, Fig. 10A). The appearance of novel bands of higher molecular weights corresponding to the addition of the His epitope establishes that Insl6 is ubiquinated *in vitro* (19). The size of the higher molecular bands indicated that less than four molecules of ubiquitin were added to one Insl6 protein, indicating that Insl6 is predominantly subjected to mono- rather than polyubiquination. A characteristic feature of ubiquination is its dependence on ATP, which is required for conjugation of ubiquitin to the substrate and for degradation of the ubiquinated protein (19). To obtain further proof of Insl6 being ubiquinated, we tested the effect of depletion of ATP on the *in vitro* degradation of Insl6. Depletion of ATP from the reticulocyte lysate mixture by addition of 2-deoxyglucose and hexokinase resulted in an inhibition of degradation of Insl6 (Fig. 10B). This sensitivity of degradation of Insl6 to ATP concentration is consistent with the Insl6 protein being ubiquinated.

Ubiquinated proteins are targeted for degradation via the proteasome pathway and/or via lysosomal degradation. To determine whether degradation of Insl6 involves the proteasome machinery, CHO cell stable-expressing mInsl6 was exposed to either clasto-lactacystin β-lactone (a proteasome inhibitor) or DMSO (vehicle), and the amount of Insl6 protein was quantified by Western blot analysis (Fig. 10C). These

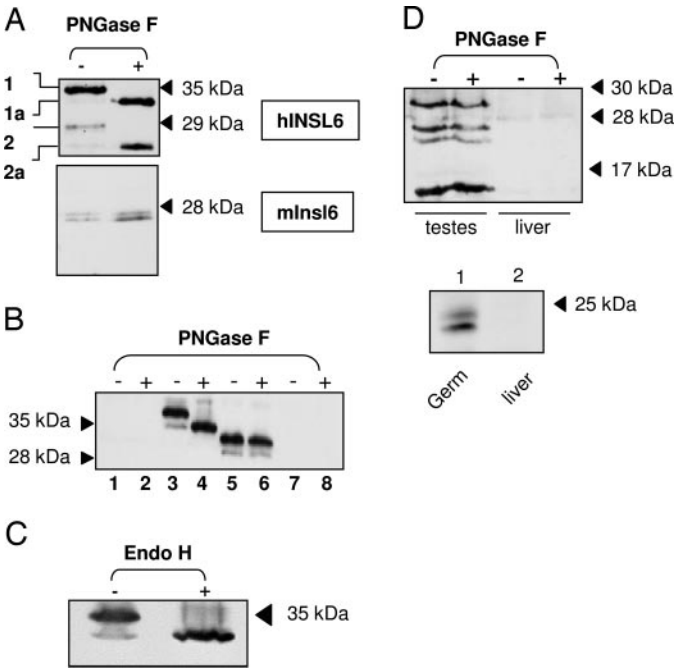

FIG. 9. Differential *N*-linked glycosylation of murine and human Insl6 proteins. A, *Top*, whole-cell lysates of CHO cells stably expressing c-*myc*-tagged human Insl6 protein were exposed to PNGase F enzyme (+) or vehicle (−), and the products were size-fractionated by SDS-PAGE electrophoresis under reducing conditions and characterized by Western blot analysis using anti c-*myc* antibody. The positions of the specific bands (1, 1a, 2, and 2a) and the molecular mass markers are indicated. Bands 1a and 2a possibly represent deglycosylated forms of bands 1 and 2, respectively. *Bottom*, Whole-cell lysates of CHO cells stably expressing c-*myc*-tagged mInsl6 protein were exposed to PNGase F enzyme (+) or vehicle (−), and the products were size-fractionated by SDS-PAGE electrophoresis under reducing conditions and characterized by Western blot analysis using anti c-*myc* antibody. The positions of the molecular mass markers are indicated. B, Protein extracts of CHO cells or Insl6-adenovirus (AdmInsl6)-infected GC2 cells were exposed to PNGase F enzyme (+) or vehicle (−), and the products were size-fractionated by SDS-PAGE electrophoresis under reducing conditions and characterized by Western blot analysis using anti c-*myc* antibody. Lanes 1 and 2, Naïve CHO cells; lanes 3 and 4, CHO cells stably expressing hInsl6; lanes 5 and 6, GC2 cells expressing adenovirally mediated mInsl6; lanes 7 and 8, naïve GC2. The cell extracts were treated with PNGase F in certain instances (lanes 2, 4, 6, and 8). The positions of the molecular mass markers are indicated. The results are representative of three independent experiments. C, Whole-cell lysates of CHO cells stably expressing c-*myc*-tagged hInsl6 protein were exposed to Endo H enzyme (+) or vehicle (−), and the products were size-fractionated by SDS-PAGE electrophoresis under reducing conditions and characterized by Western blot analysis using anti c-*myc* antibody. The position of the molecular mass marker is indicated. D, *Top*, aliquots of mouse testis or liver whole-cell extracts were exposed to PNGase F enzyme (+) or vehicle (−), and the products were size-fractionated by SDS-PAGE electrophoresis under reducing conditions and characterized by Western blot analysis using anti-Insl6 antibody (EE). The positions of the molecular mass markers are indicated. *Bottom*, Aliquots of whole-cell extracts of either mouse germ cells (lane 1) or liver (lane 2) were size-fractionated by SDS-PAGE electrophoresis under reducing conditions and characterized by Western blot analysis using anti-Insl6 A peptide antibody (Phoenix Pharmaceuticals). The position of the molecular mass marker is indicated.

results revealed that treatment with clasto-lactacystin β-lactone resulted in increase in the steady levels of Insl6 in these cells, suggesting that the degradation of Insl6 involves the proteasome pathway. To further explore this possibility, clasto-lactacystin β-lactone or DMSO was added into an *in vitro* translation system designed to translate the mInsl6 protein. As shown in Fig 10D, addition of clasto-lactacystin β-lactone partially inhibited the degradation of the *in vitro*-synthesized Insl6. Similar results were obtained via pulse chase experiments (Fig. 10E), wherein exposure of CHO cells stably expressing Insl6 to clasto-lactacystin β-lactone resulted in a modest prolongation of the half-life of Insl6 from 45–80 min. The lack of total inhibition of Insl6 degradation after blockade of the proteasome pathway prompted an investigation of alternate routes for intracellular protein degradation. Thus, exposure of Insl6 stably expressing CHO cells to the lysosome inhibitors chloroquine resulted in a more pronounced abrogation of degradation of Insl6, indicating the participation of the lysosomal pathway in Insl6 degradation (Fig. 10E).

Discussion

Insl6 is a recently identified member of the insulin/relaxin gene superfamily whose biological role is yet to be defined (13–15). The goal for the present study was to gain insights into the biological actions of Insl6. The main findings of the current study are that Insl6 is a secreted protein expressed in the germ cells of the testis; Insl6 undergoes posttranslational modifications including prohormone processing, disulfide bond formation, *N*-linked glycosylation, and ubiquitination; and Insl6 is a target for furin action.

Our results indicate that the site of maximal expression of Insl6 is the germ cell of the testis and that expression of Insl6 is restricted to the midpachytene spermatocytes, secondary spermatocytes, and round spermatids stages of germ cell maturation. Although a previous report (15) had also concluded, on the basis of *in situ* hybridization studies, that Insl6 was predominantly expressed in the germ cell of the testis, Hsu (13) reached the disparate conclusion that Leydig cells are the exclusive site of expression of Insl6. The reason(s) for the discrepancy between the results of the immunohistochemical experiments conducted by Hsu and those of the current study is not clear. Although our results do not exclude the possibility that the Leydig cell may also be a site of expression of Ins6, our results do establish unequivocally that the germ cell is the principal site of Insl6 expression in the adult testis. This conclusion is based on multiple lines of evidence including immunohistochemistry, expression profile of Insl6 mRNA in models of germ cell depletion, and ontogenic profile of mRNA expression in the testis.

Characterized members of the insulin/relaxin superfamily all are secreted proteins with signal peptides in their primary structure and intra- and intermolecular cysteine-linked disulfide bonds in the mature protein. In the present study, we demonstrate that Insl6 is also a secreted protein containing disulfide bonds with intracellular localization to the ER and Golgi. Secretion of Insl6 was confirmed in both CHO and GC2 cells. This secretion could be blocked by BFA treatment, suggesting that Insl6 is secreted through a classic secretory pathway. Ectopic expression of Insl6 in either CHO or GC2 cells resulted in two major bands. In cell lysates, the predominant Insl6 band was approximately 28 kDa in size.

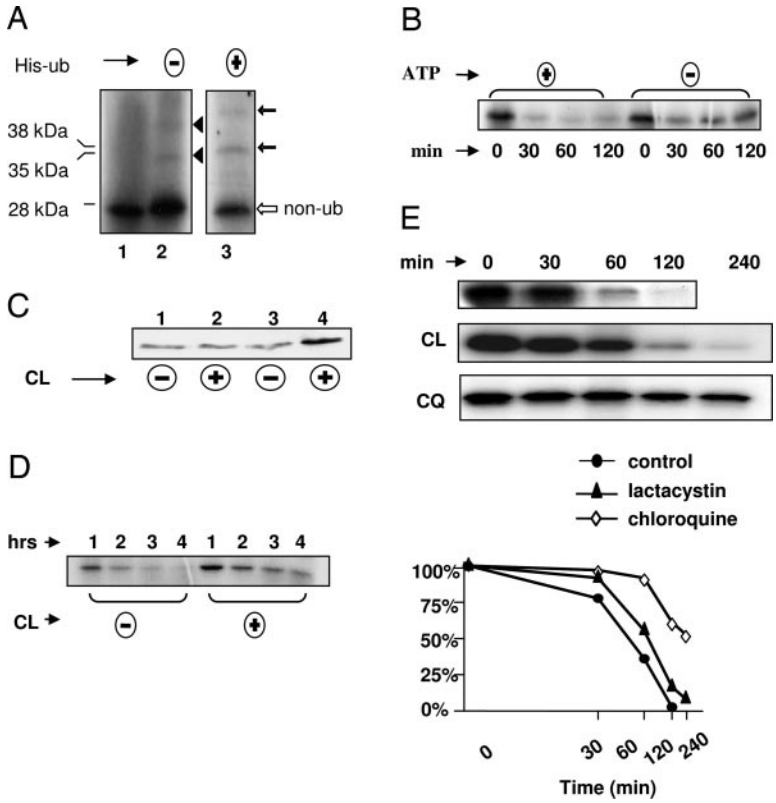

FIG. 10. Insl6 is an ubiquinated protein. A, *In vitro* ubiquination of mouse Insl6. Coupled *in vitro* transcription-translation reaction using wheat germ extract (lane 1) or reticulocyte lysate (lanes 2 and 3) was used to synthesize [^{35}S] cysteine-labeled mInsl6 in the absence (−) or presence (+) of His-tagged ubiquitin. The products were size fractionated via SDS-PAGE electrophoresis and visualized by autoradiography. The position of putatively ubiquinated higher molecular mass products are indicated in both the reaction without (◀) and with (←) His-ubiquitin. Note the apparent increase in molecular mass of the bands in the His-ubiquitin reactions. B, Degradation of mInsl6 *in vitro* is ATP dependent. mInsl6 protein was expressed in a transcription-translation-coupled system where either ATP (+) or ATP-depleting mixture (−) was added 30 min after initiation of the reaction. Aliquots of the reaction at the indicated time-periods were analyzed by SDS-PAGE and autoradiography. C, Degradation of Insl6 is blocked by proteasome inhibitors *in vivo*. CHO cells stably expressing c-*myc*-tagged mInsl6 were either exposed to vehicle (−) or 5 μM clasto-lactacystin-β-lactone (CL) (+), and cells harvested after 4 (lanes 1 and 2) or 24 (lanes 3 and 4) h. The cell lysates were analyzed by Western blot using anti-myc antibody. D, Degradation of Insl6 is blocked by proteasome inhibitors *in vitro*. Coupled *in vitro* transcription/translation of Insl6 using reticulocyte lysates performed for the indicated time (hours) in the presence of either vehicle (−) or 5 μM clasto-lactacystin-β-lactone (Clasto-L) (+). The reaction products were size-fractionated via SDS-PAGE and autoradiographed. E, Stability of Insl6 in the presence of proteasomal or lysosomal inhibitor. CHO cells stably expressing c-*myc*-tagged mInsl6 were exposed to vehicle, proteasomal inhibitor [clasto-lactocysteine (CL), 10 μM], lysosomal inhibitors [0.2 mM chloroquine (CQ) or 1 μM bafilomycin (Baf)]. mInsl6 protein expressed in these cells was pulse labeled using [^{35}S] cysteine and chased with unlabeled cysteine. At the indicated time points, cells were harvested, immunoprecipitated with anti-myc (9E10) monoclonal antibody, and analyzed by SDS-PAGE as described in *Materials and Methods*. For a graphical representation of the results, the intensity of the specific bands was quantified by densitometry, and the results were depicted as relative to intensity of the band at time 0 designated as 100%. The x-axis is depicted in log and the y-axis in linear scale.

In contrast in the supernatant, the dominant band was a doublet of 6/8 kDa (putative A peptide) in size under reducing conditions and 12/14 kDa (putative A + B peptide) under nonreducing conditions. Our results establish for the first time that Insl6, like other members of the insulin family, is processed from precursor (28 kDa) to mature protein (14 kDa) and that the mature protein is linked by disulfide bonds. BFA treatment blocked the secretion of Insl6 in both CHO and GC2 cells, suggesting that the 8-kDa Insl6 peptide is processed and secreted and does not result from nonspecific degradation of dead cells.

Mouse prepro-Insl6 has 191 aa. Because this protein was fused with the myc-His tag, the total number of aa for the fused protein is 22,5 and the predicted size of this protein on SDS-PAGE is approximately 25 kDa for prepro-mInsl6 and 22 kDa for pro-mInsl6. Our results indicate that the putative mouse pro-Insl6 migrated as a 28-kDa doublet, 11–14% larger than expected. At the present time, the reason(s) for the Insl6 precursor migrating as a doublet is not clear. We ruled out the possibility of incomplete reduction of disulfide bonds resulting in oxidized and reduced forms of the protein by treating the protein samples with the alkylating agent iodoacetamide before electrophoresis (data not shown). However, this treatment failed to alter the doublet configuration of the mouse pro-Insl6 protein, indicating that the doublet configuration is not consequent to incomplete reduction or reoxidization of SH groups in the peptide. We excluded the possibility of glycosylation of the murine Insl6 (Fig. 9, A, B, and D) as being a reason for the doublet or the discrepancy in size. In addition to posttranslational modifications and incomplete reduction of disulfide bonds, excess positive or negative charged residues can result in aberrant mobility of

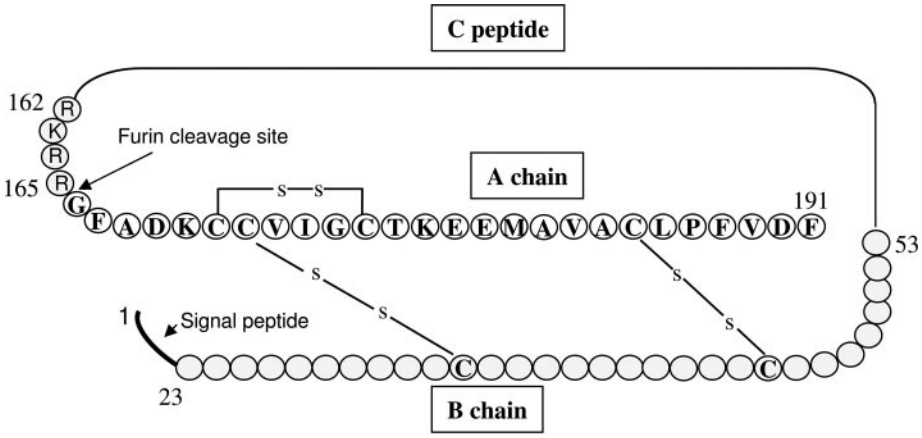

FIG. 11. Mouse Insl6 protein. The predicted signal peptide (*italicized*), B chain (*boxed*), C chain (*gray*), and A chain (*boxed*) are specified. The putative locations of the disulfide bonds and furin cleavage site are indicated.

***MKQLCCSCLLWLGLLLTPFSRE*EEEESRPRKLCGRHL**
LIEVIKLCGQSDWSREEMEEQSPMTQFFPHYSRKGK
AFNPHPSSSAWRRFTNPVPAGVSQKKGTHTWEPQS
LPDYQFEKTELLPKARVFSYHSGKPYVKSVQLQKKS
TNKMNTFRSLFWGNHSQRKRR**GFADKCCVIGCTKE**
EMAVACLPFVDF

a protein on SDS-PAGE (23, 24). A Glu-rich region (EEEEE) is present (aa 22–26) in the mouse Insl6 peptide. Glu-rich regions have been shown to interfere with protein mobility on SDS-PAGE, resulting in an artifactual increase in estimation of molecular weight on SDS-PAGE (25), and it is possible that such a phenomenon may be contributing to the slower than predicted mobility of the mouse Insl6 protein on SDS-PAGE. Total aa for the myc-his-tagged human Insl6 is 249 aa, and the size of the human prepro- and pro-Insl6 is predicted to be approximately 28 and 25 kDa, respectively. Our results indicate that the size of the human prepro/pro-Insl6 is approximately 35 kDa before deglycosylation and 32 kDa after deglycosylation. Hence, the size of the human Insl6 is approximately 11% larger than the predicted size. We hypothesize that similar to the mouse protein, this discrepancy in molecular size could be due to excess negative charge of tandem glutamic acid residues located at aa 56–58 and aa 102–103.

The mammalian PC cadre of proteins include furin/PACE, PC1/PC3, PC2, PC4, PACE4, PC5/PC6, PC7/PC8/LPC, SKI/S1P, and NARC-1/PCSK9. CHO cells have been demonstrated to express furin and PC7 and SKI-1 (26–28), and LoVo cells are deficient in furin but express other PCs such as PC7 and PACE4 (29, 30). Our results with the furin inhibitor Dec-RVKR-CMK and furin-deficient LoVo cells establish that Insl6 is a target for furin action and that furin is one of the PCs responsible for the 6-/8-kDa doublet configuration of the mature protein on gel electrophoresis. Our results also establish the identity of one of the cleavage sites (RKRR, aa 162–165) of the mInsl6 peptide. Experiments using ectopic expression of furin indicate that this site is a target for furin action. Furthermore, differences in the size of the secreted protein after inhibition of furin activity or mutation of this cleavage site predicts that this site must also be a site for action by nonfurin PC(s). It is noteworthy that the molecular weight profiles of proteins synthesized via ectopic expression of Insl6 in GC2 cells were similar to that observed with ectopic expression in CHO cells, suggesting similarity in the Insl6-directed PC activity in these two cell types. The demonstration of the secretory status of Insl6 could provide clues to the cellular targets of Insl6 action. Thus, in addition to possible autocrine actions on the germ cell, the physical proximity of the germ cell to the Sertoli cell renders the Sertoli cell a likely candidate for Insl6 action. In this regard, the demonstration of Insl6 expression in the brain (31) suggests biological actions of Insl6 outside the testis.

Our studies indicate that Insl6 undergoes other posttranslational modifications such as ubiquitination and *N*-glycosylation in a species-specific manner. Our results establish that the human Insl6 precursor is *N*-glycosylated, consistent with the *in silico* prediction. In contrast, despite the presence of a computer-predicted putative *N*-glycosylation site in the mouse Insl6 gene, we were unable to demonstrate *N*-glycosylation of the murine Insl6 protein in either CHO or GC2 cells and in mouse testis extracts. The functional significance of this differential species-specific glycosylation status of the Insl6 protein remains to be elucidated. Protein ubiquitination is an important form of covalent modification that regulates various cellular processes including cell division, growth, communication/signaling, movement, and death/apoptosis (32). The ubiquitin system in the testis plays a role in sperm cell differentiation and the control of cell cycle during spermatogenesis, and mutations in components of the ubiquitin system result in male infertility (33). The ubiquitin proteolytic system has generally been regarded as a cytosolic or nuclear pathway. However, recent studies have identified the presence of ubiquitin and ubiquitin-activating enzyme associated with a post-ER/pre-Golgi compartment with the intracellular degradation of certain secreted proteins (*e.g.* preproparathyroid hormone-related protein) being dependent on ubiquination. It is further postulated that ubiquination plays a role in ER quality control of misfolded

molecules during the synthesis of these proteins (19, 34). A single protein can be modified on one or more lysines with a limited number (<4) of ubiquitin molecules (monoubiquination) or with lysine-linked chains of ubiquitin (polyubiquination) (35, 36). Although polyubiquinated proteins are targeted for degradation via the proteasome, monoubiquinated proteins are preferentially degraded in the lysosome. With respect to Insl6, inhibition of either the proteasomal pathway or lysosomal enzymatic activity resulted in prolongation of the half-life of the protein, although the effect of lysosomal inhibition was more dramatic and complete. How can the half-life of the Insl6 protein be apparently affected by perturbation of both the proteasome and the lysosomal pathways? We propose that Insl6 is monoubiquinated and that the primary mode of degradation is by the lysosomal pathway. We hypothesize that the partial effect of proteasome inhibitors on Insl6 degradation is the indirect result of lower cellular levels of ubiquitin that can be induced by proteasome inhibitors (37, 38) and does not reflect a direct role of the proteasome in Insl6 degradation. A caveat in our results is that our results regarding ubiquination of Insl6 were obtained exclusively using an *in vitro* system. Further studies will be required to confirm the presence, characteristics, and biological role of *in vivo* ubiquination of the Insl6 protein.

In conclusion, our results indicate that Insl6 is expressed in the germ cells of the testis. Data presented in the current study demonstrate that Insl6 is a disulfide-linked secreted protein using the classic secretion pathway that undergoes processing from preprohormone to mature hormone, with furin playing a role in this processing. Insl6 is also subjected to ubiquitination and *N*-glycosylation in a species-specific manner.

Acknowledgments

We acknowledge Drs. Serge Nef and Luis F. Parada (University of Texas, Southwestern Medical Center, Dallas) for their generous gift of murine fetal testes RNA, Alnawaz Rehemtulla (University of Michigan, Ann Arbor) for plasmid-expressing furin, and the assistance of Dr. Simon C. Watkins, Director (Center for Biologic Imaging and the Cell Image Core, Center for Reproductive Physiology, University of Pittsburgh).

Received April 19, 2006. Accepted August 14, 2006.

Address all correspondence and requests for reprints to: Ram K. Menon, M.D., University of Michigan Medical School, 1205 Medical Professional Building Box 0718, 1500 East Medical Center Drive, Ann Arbor, Michigan 48109-0718. E-mail: rammenon@umich.edu.

This work was supported by the National Institutes of Health [Grants HD HD044436 and DK49845 (to R.K.M.) and T32DK07729], by the Children's Hospital of Pittsburgh (Renzeihausen Fund), and by the Vira I. Heinz Foundation. This work was also supported in part by the Michigan Diabetes Research and Training Center Grant (P60DK-20572) from the National Institute of Diabetes and Digestive and Kidney Diseases.

The authors have nothing to disclose.

References

1. **LeRoith D, Shiloach J, Roth J, Lesniak MA** 1980 Evolutionary origins of vertebrate hormones: substances similar to mammalian insulins are native to unicellular eukaryotes. Proc Natl Acad Sci USA 77:6184–6188
2. **Konopinska D, Rosinski G, Sobotka W** 1992 Insect peptide hormones, an overview of the present literature. Int J Pept Protein Res 39:1–11
3. **Smit AB, van Marle A, van Elk R, Bogerd J, vanHeerikhuizen H, Geraerts WP** 1993 Evolutionary conservation of the insulin gene structure in invertebrates: cloning of the gene encoding molluscan insulin-related peptide III from *Lymnaea stagnalis*. J Mol Endocrinol 11:103–113
4. **Ishizaki H, Suzuki A** 1994 The brain secretory peptides that control moulting and metamorphosis of the silkmoth, *Bombyx mori*. Int J Dev Biol 38:310
5. **Duret L, Guex N, Peitsch MD, Bairoch A** 1998 New insulin-like proteins with atypical disulfide bond pattern characterized in *Caenorhabditis elegans* by comparative sequence analysis and homology modeling. Genome Res 8:348–353
6. **Reinecke M, Eppler E, David I, Georges D** 1999 Immunohistochemical evidence for the presence, localization and partial coexistence of insulin, insulin-like growth factor I and relaxin in the protochordate *Ciona intestinalis*. Cell Tissue Res 295:331–338
7. **Wilkinson T, Speed T, Tregear G, Bathgate R** 2005 Evolution of the relaxin-like peptide family. BMC Evol Biol 5:14
8. **Burkhardt E, Adham IM, Brosig B, Gastmann A, Mattei MG, Engel W** 1994 Structural organization of the porcine and human genes coding for a Leydig cell-specific insulin-like peptide (LEY I-L) and chromosomal localization of the human gene (INSL3). Genomics 20:13–19
9. **Zimmermann S, Steding G, Emmen JM, Brinkmann AO, Nayernia K, Holstein AF, Engel W, Adham IM** 1999 Targeted disruption of the Insl3 gene causes bilateral cryptorchidism. Mol Endocrinol 13:681–691
10. **Chassin D, Laurent A, Janneau JL, Berger R, Bellet D** 1995 Cloning of a new member of the Insulin gene superfamily (INSL4) expressed in human placenta. Genomics 29:465–470
11. **Koman A, Cazaubon S, Couraud PO, Ullrich A, Strosberg AD** 1996 Molecular characterization and in vitro biological activity of placentin, a new member of the insulin gene family. J Biol Chem 271:20238–20241
12. **Conklin D, Lofton-Day CE, Haldeman BA, Ching A, Whitmore TE, Lok S, Jaspers S** 1998 Identification of INSL5, a new member of the insulin superfamily. Genomics 60:50–56
13. **Hsu SY** 1999 Cloning of two novel mammalian paralogs of relaxin/insulin family proteins and their expression in testis and kidney. Mol Endocrinol 13:2163–2174
14. **Kasik J, Muglia L, Stephan DA, Menon RK** 2000 Identification, chromosomal mapping, and partial characterization of mouse Insl6: a new member of the insulin family. Endocrinology 141:458–461
15. **Lok S, Johnston DS, Conklin D, Lofton-Day CE, Adams RL, Jelmberg AC, Whitmore TE, Schrader S, Griswold MD, Jaspers SR** 2000 Identification of INSL6, a new member of the insulin family that is expressed in the testis of the human and rat. Biol Reprod 62:1593–1599
16. **Liu C, Eriste E, Sutton S, Chen J, Roland B, Kuei C, Farmer N, Jornvall H, Sillard R, Lovenberg TW** 2003 Identification of relaxin-3/INSL7 as an endogenous ligand for the orphan G-protein-coupled receptor GPCR135. J Biol Chem 278:50754–50764
17. **Hardy S, Kitamura M, Harris-Stansil T, Dai Y, Phipps ML** 1997 Construction of adenovirus vectors through Cre-lox recombination. J Virol 71:1842–1849
18. **Yu JH, Schwartzbauer G, Kazlman A, Menon RK** 1999 Role of the Sp family of transcription factors in the ontogeny of growth hormone receptor gene expression. J Biol Chem 274:34327–34336
19. **Meerovitch K, Wing S, Goltzman D** 1997 Preproparathyroid hormone-related protein, a secreted peptide, is a substrate for the ubiquitin proteolytic system. J Biol Chem 272:6706–6713
20. **Chomczynski P, Sacchi N** 1987 Single-step method of RNA isolation by acid guanidinium thiocyanate-phenol-chloroform extraction. Anal Biochem 162: 156–159
21. **Gibson UE, Heid CA, Williams PM** 1996 A novel method for real time quantitative RT-PCR. Genome Res 6:995–1001
22. **PE Biosystems** 1997 ABI Prism 7700 Sequence Detection System, relative quantitation of gene expression: PE Applied Biosystems user bulletin 2. Foster City, CA: PE Biosystems
23. **Hu CC, Ghabrial SA** 1995 The conserved, hydrophilic and arginine-rich N-terminal domain of cucumovirus coat proteins contributes to their anomalous electrophoretic mobilities in sodium dodecylsulfate-polyacrylamide gels. J Virol Methods 55:367–379
24. **Armstrong DJ, Roman A** 1993 The anomalous electrophoretic behavior of the human papillomavirus type 16 E7 protein is due to the high content of acidic amino acid residues. Biochem Biophys Res Commun 192:1380–1387
25. **Iakoucheva LM, Kimzey AL, Masselon CD, Smith RD, Dunker AK, Ackerman EJ** 2001 Aberrant mobility phenomena of the DNA repair protein XPA. Protein Sci 10:1353–1362
26. **Nour N, Basak A, Chretien M, Seidah NG** 2003 Structure-function analysis of the prosegment of the proprotein convertase PC5A. J Biol Chem 278:2886–2895
27. **Gu M, Rappaport J, Leppla SH** 1995 Furin is important but not essential for the proteolytic maturation of gp160 of HIV-1. FEBS Lett 365:95–97
28. **Pullikotil P, Vincent M, Nichol ST, Seidah NG** 2004 Development of protein-based inhibitors of the proprotein of convertase SKI-1/S1P: processing of SREBP-2, ATF6, and a viral glycoprotein. J Biol Chem 279:17338–17347
29. **Takahashi S, Nakagawa T, Kasai K, Banno T, Duguay SJ, Van de Ven WJ, Murakami K, Nakayama K** 1995 A second mutant allele of furin in the processing-incompetent cell line, LoVo. Evidence for involvement of the homo B domain in autocatalytic activation. J Biol Chem 270:26565–26569
30. **Seidah NG, Hamelin J, Mamarbachi M, Dong W, Tardos H, Mbikay M,**

Chretien M, Day R 1996 cDNA structure, tissue distribution, and chromosomal localization of rat PC7, a novel mammalian proprotein convertase closest to yeast kexin-like proteinases. Proc Natl Acad Sci USA 93:3388–3393
31. **Brailoiu GC, Dun SL, Yin D, Yang J, Chang JK, Dun NJ** 2005 Insulin-like 6 immunoreactivity in the mouse brain and testis. Brain Res 1040:187–190
32. **Hershko A, Ciechanover A** 1998 The ubiquitin system. Annu Rev Biochem 67:425–479
33. **Sutovsky P** 2003 Ubiquitin-dependent proteolysis in mammalian spermatogenesis, fertilization, and sperm quality control: killing three birds with one stone. Microsc Res Tech 61:88–102
34. **Yeung S, Chen S, Chan L** 1996 Ubiquitin-proteasome pathway mediates intracellular degradation of apolipoprotein B. Biochemistry 35:13843–13848
35. **Hicke L** 2001 Protein regulation by monoubiquitin. Nat Rev Mol Cell Biol 2:195–201
36. **Weissman AM** 2001 Themes and variations on ubiquitylation. Nat Rev Mol Cell Biol 2:169–178
37. **Schubert U, Ott DE, Chertova EN, Welker R, Tessmer U, Princiotta MF, Bennink JR, Krausslich HG, Yewdell JW** 2000 Proteasome inhibition interferes with gag polyprotein processing, release, and maturation of HIV-1 and HIV-2. Proc Natl Acad Sci USA 97:13057–13062
38. **Mimnaugh EG, Chen HY, Davie JR, Celis JE, Neckers L** 1997 Rapid deubiquitination of nucleosomal histones in human tumor cells caused by proteasome inhibitors and stress response inducers: effects on replication, transcription, translation, and the cellular stress response. Biochemistry 36:14418–14429

***Endocrinology* is published monthly by The Endocrine Society (http://www.endo-society.org), the foremost professional society serving the endocrine community.**